First cycle simulations of the Honigmann process with $LiBr/H_2O$ and $NaOH/H_2O$ as working fluid pairs as a thermochemical energy storage

Anna Jahnke*, Lia Strenge, Christian Fleßner, Niklas Wolf, Tim Jungnickel and Felix Ziegler

Fachgebiet Maschinen- und Energieanlagentechnik, Institut für Energietechnik, Technische Universität Berlin, KT2, Marchstraße 18, Berlin 10587, Germany

Abstract

A thermochemical energy storage invented in the 19th century, the so-called 'Honigmann process', is reconsidered for the storage of renewable energies or waste heat. In this work, one basic process option of charging with the input of low-grade heat and discharging with the release of mechanical work is studied. A fundamental model based on transient energy and mass balances was implemented with the help of the modelling language Modelica. First simulation results indicate a relatively constant power output in spite of the non-steady-state nature of the process.

Keywords: thermochemical energy storage; heat storage; fireless locomotive; sorption technology; renewable energies

*Corresponding author:
anna.jahnke@tu-berlin.de

Received 18 January 2013; revised 12 March 2013; accepted 20 March 2013

1 INTRODUCTION

In 1883, Moritz Honigmann invented a process and filed a patent of the so-called 'fireless locomotives' [1, 2]. In the following years, several machines of this type were built and experiments were done in short-distance railway systems, e.g. close to Aachen, Germany [3–7]. Even though his tests were successful, the invention did not find wide distribution. Honigmann made several proposals for process optimizations, which can be found in Honigmann [8, 9], for example. He used sodium hydroxide and water as working fluids. In parallel, Emile Lamm made the same invention with a different working pair (H_2O/NH_3) [10].

Later, Raymond D'Equevilley-Montjustin used this idea to power submarine boats. Corresponding patents can be found in Lamm [11] and D'Equevilley-Montjustin [11, 12].

Isshiki *et al.* discussed other applications of this process at the end of the 20th century and called it 'concentration difference energy system' [13, 14]. This group built several Honigmann machines with $LiCl/H_2O$ as the working pair to run a tricycle [15], for example. Scenarios for large-scale realizations as well as multistage machines or combinations with common Rankine cycles were proposed.

Today, the process could be used for the storage of renewable energies. In general, the storage can be charged with the input of heat or mechanical work and discharged with the release of heat, cold or mechanical work [16]. This flexibility is the major advantage of the process compared with the other storage technologies as well as compared with waste heat driven Rankine cycles. Another advantage is the absence of self-discharge (with the exception of minor heat losses).

Even though there have been quite some activities on the process in the past, only little data exist. A profound analysis of the process is missing so far. This was the reason to develop the presented model. It is now possible to simulate the dynamic behaviour of the process to investigate operating and control strategies and the choice of different working fluid pairs. It might also be used to analyze and discuss the existing data of the 19th century with up to date scientific knowledge.

2 DESCRIPTION OF THE PROCESS

In this section, the working principle is described. The discharging process is based on two basic physical effects (Figure 1, left side).

International Journal of Low-Carbon Technologies 2013, 8, i55–i61

doi:10.1093/ijlct/ctt022

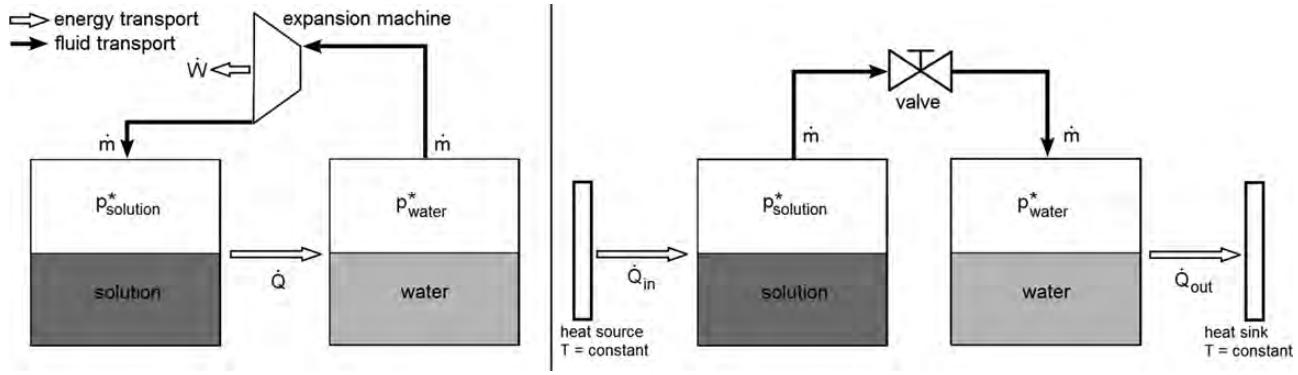

Figure 1. *Flow scheme of the process (left, discharging; right, charging).*

(1) The first effect is the vapour pressure depression of an aqueous solution compared with the working fluid (water). Due to the difference in the vapour pressure, an expansion machine can be operated by steam flowing from a water vessel to a solution vessel at an even higher temperature.
(2) The second essential effect is the occurrence of heat of absorption which can be recovered. The water vapour is absorbed in the solution and heat of absorption is set free. This heat is transferred to the water vessel to evaporate more water and the expansion continues.

The solution becomes more and more diluted until the vapour pressure difference becomes too small to run the expansion machine. This is the time when the storage needs to be recharged. Recharging can be accomplished with the input of heat to desorb the water out of the aqueous solution (Figure 1, right side). To recover the water and maintain a closed cycle, the water vapour will be condensed at a lower temperature.

3 MODEL AND SIMULATION ASSUMPTIONS

The three main components are modelled and the physical models are implemented into a simulation tool (modelling language Modelica [17] with simulation environment Dymola [18]):

- vessel with a heat exchanger containing aqueous solution,
- vessel with a heat exchanger containing water and
- expansion machine.

There is also a valve in this path, which can be opened or closed.

The vessels are modelled as completely stirred tank reactors with only one temperature, mass fraction and the corresponding vapour pressure. Effects of superheating or subcooling are not considered. The liquid solution and water in the vessels are assumed as incompressible.

The energy balance for the solution vessel is given by Equation (1). The change of the inner energy of the solution U_{sol} equals the enthalpy flow $\dot{H}_{vap}$ of the water vapour and the heat flow $\dot{Q}$:

$$\frac{dU_{sol}}{dt} = \dot{H}_{vap} + \dot{Q}. \quad (1)$$

This includes the neglection of the kinetic and potential energy as well as of the heat capacities of the vessels etc. With the assumption that the amount of the vapour in the solution vessel is negligible when compared with the liquid, and with the additional information that for the liquid fluid, the product of pressure and specific volume is much smaller than the specific inner energy ($p \cdot v \ll u$), we get $h_{sol} = u_{sol}$ and write:

$$\frac{d(h_{sol} \cdot m_{sol})}{dt} = h_{vap} \cdot \dot{m}_{vap} + \dot{Q}. \quad (2)$$

The mass of the solution m_{sol} increases or decreases with the incoming or the outgoing mass flow of the working fluid $\dot{m}_{vap}$:

$$\frac{dm_{sol}}{dt} = \dot{m}_{vap}. \quad (3)$$

In the case of absorption, the specific enthalpy of the water vapour h_{vap} depends on the expansion process in the turbine. We start with the saturated vapour at evaporator pressure and assume expansion with a defined isentropic efficiency η_{isen}:

$$\eta_{isen} = \frac{h_{in} - h_{out}}{h_{in} - h_{out,isen}}. \quad (4)$$

The pressure at the end of the expansion is the vapour pressure of the solution. The expanded vapour has a liquid and a gas component. In Equation (4), h_{in} and h_{out} are both specific enthalpies of the vapour (h_{vap}). The term h_{in} is the enthalpy of the vapour leaving the evaporator and flowing into the expansion machine, and the term h_{out} is the enthalpy of the vapour flowing out of the expansion machine and entering the

absorber [h_{vap} in Equation (2)]. The term $h_{out,isen}$ is the enthalpy in the case of isentropic expansion.

In the case of desorption, the enthalpy h_{vap} equals the enthalpy of the water vapour at the vapour pressure and the temperature of the solution.

During the absorption, the heat of absorption is transferred to the water vessel. For the regeneration process, heat of desorption is needed to regenerate the solution. It represents the driving energy of the process.

The energy balance for the water vessel is given by Equation (5) and is treated in the same way as for the solution vessel:

$$-\frac{\mathrm{d}U_{water}}{\mathrm{d}t} = -\dot{H}_{vap} + \dot{Q}. \tag{5}$$

Comparable with Equation (2), the inner energy U_{water} is substituted by the enthalpy of the condensate $h_{water} \cdot m_{water}$, and the enthalpy flow $\dot{H}_{vap}$ is replaced by $h_{vap} \cdot m_{vap}$. The term h_{vap} is the specific enthalpy of the incoming or the outgoing water vapour flow. During evaporation, it is equal to the enthalpy of the saturated water vapour at evaporator temperature. For the condensation, it is the outgoing vapour of the solution vessel with the equilibrium temperature of the solution.

The mass balance for the water vessel is comparable with that of the solution vessel.

The expansion machine is modelled with a simple form of the Stodola equation (e.g. Sigloch [19], p. 272) which is made for turbines with constant rotational speed:

$$\frac{\dot{m}_{vap}^2}{\dot{m}_{vap,N}^2} = \frac{p_{in}^2 - p_{out}^2}{p_{in,N}^2 - p_{out,N}^2}. \tag{6}$$

In this equation, the vapour mass flow $\dot{m}_{vap}$ and in- and outlet pressure p_{in} and p_{out} are set in relation to the corresponding 'nominal' values. If the pressures in the vessels change, the Stodola equation describes how this influences the mass flow rate through the turbine. In a more elaborate version of the model, the inlet temperature can also be taken into account [20]. For positive displacement machines, Equation (6) may be altered.

Finally, for the expansion machine, the mechanical power output $\dot{W}$ is:

$$\dot{W} = -(h_{in} - h_{out}) \cdot \dot{m}_{vap}. \tag{7}$$

The heat source and sink during the charging process are modelled as constant temperature baths. In real applications, the source and the sink temperatures exhibit a glide, which, however, does not change the fundamental findings of our calculations.

All heat exchange processes are modelled with a constant heat transfer capacity and the temperature difference ΔT between the components [Equation (8)]. The 'heat transfer capacity' or the 'UA value' G is defined as the product of the overall heat transfer coefficient U and the heat exchanger surface A.

$$\dot{Q} = U \cdot A \cdot \Delta T = G \cdot \Delta T. \tag{8}$$

The process proceeds in four consecutive phases:

(1) Discharging the storage (Figure 1, left side),
(2) Cooling of the vessels until the pressures are equal (Figure 1, right side),
(3) Charging the storage (Figure 1, right side) and
(4) Heating of the vessels to the initial discharging conditions (Figure 1, right side).

The full model and all assumptions are described in detail in Strenge [21].

Simulations with two different working pairs are carried out: aqueous lithium bromide solution and water ($LiBr/H_2O$) and sodium hydroxide solution and water ($NaOH/H_2O$). The reason is that the sodium hydroxide solution was used in the 19th century by Honigmann *et al.* to carry out test runs for his invention and that a lithium bromide solution will be used at Technische Universität Berlin to run an experimental plant. Other working pairs such as H_2O/NH_3 or Ionic liquids/H_2O could also be used.

Thermodynamic property data are from Pátek and Klomfar [22] ($LiBr/H_2O$) and Olsson *et al.* [23] ($NaOH/H_2O$), and the Modelica media library (based on [24]) is used for water.

The initial temperatures (120°C for the solution and 110°C for water) and pressure (0.19 bar for the solution) are identical for both simulations. This results in different starting mass fractions for the solutions, as the vapour pressures are different. All other boundary conditions are identical for both working pairs. In both cases, 3.6 kg of water is expanded. The heat source for regeneration is set to 120°C and the heat sink for condensation to 40°C (Table 1). For the heat transfer capacity between the vessels during the discharging phase, it is defined that 5 kW thermal power should be transferred at a temperature difference of 10 K. During the charging phase, heat transfer capacities are chosen so that in the last phase of charging, a minimal temperature difference of 3 K is achieved. From absorption cooling machines, it is known that these values are technically feasible. The nominal vapour mass flow of the expansion machine is set to 2 g/s at a nominal inlet pressure of 1.43 bar and a nominal outlet pressure of 0.19 bar. The nominal vapour flow corresponds to 5 kW thermal power, since this amount is needed for the evaporation of the water. The nominal in- and outlet pressures are the vapour pressures corresponding to the initial temperatures of water and solution.

4 RESULTS AND DISCUSSION

Results of the simulations for $LiBr/H_2O$ are shown in Figures 2–6. First, these results are explained. The comparison

Table 1. *Set of parameters for the simulations*

	Component	Parameter	Symbol	Value
1. Discharging	Water vessel	Start mass	m_{water}	4.6 kg
		Start temperature	T	110°C
	Solution vessel	Start mass	m_{sol}	19.8 kg
		Start temperature	T	120°C
		Start mass fraction $LiBr/H_2O$	ξ_{LiBr/H_2O}	0.650 kg_{LiBr}/kg_{sol}
		Start mass fraction $NaOH/H_2O$	ξ_{NaOH/H_2O}	0.617 kg_{NaOH}/kg_{sol}
	Expansion machine	Isentropic efficiency	η_{isen}	0.5
		Nominal vapour mass flow	$\dot{m}_{vap,N}$	2 g/s
		Nominal inlet pressure	$p_{in,N}$	1.43 bar
		Nominal outlet pressure	$p_{out,N}$	0.19 bar
	Between the vessels	Heat transfer capacity	G	500 W/K
2. Cooling	Heat sink at the water vessel	Temperature	T	40°C
3. Charging	Heat source at the solution vessel	Temperature	T	120°C
	At the solution/water vessel	Heat transfer capacity	G	700 W/K/2200 W/K
4. Heating	Heat source at the water vessel	Temperature	T	110°C
	Heat source at the solution vessel	Temperature	T	120°C
	At the solution/water vessel	Heat transfer capacity	G	700 W/K/2200 W/K

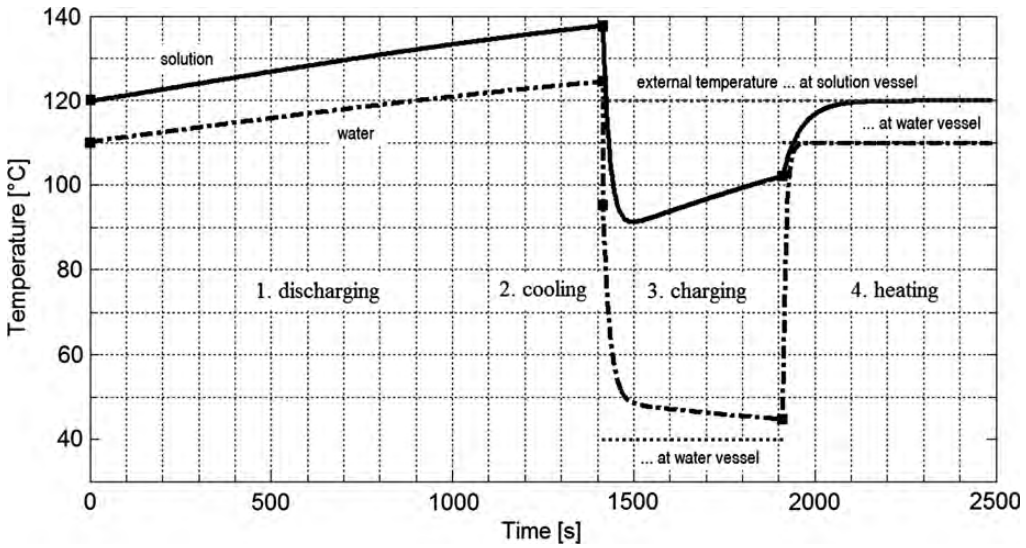

Figure 2. *Temperature of water and solution.*

of the two working pairs is done later in the text. In the discussion, a focus is set on the discharging phase.

In Figure 2, the temperatures of the working fluids are plotted over time. The external temperature baths are also depicted. In the first phase (discharging), no external heat source or sink is needed. The beginning of each phase is marked by two little squares.

(1) Discharging: the heat of absorption is higher than the heat of evaporation. The heat 'produced' by absorption in the solution vessel is thus higher than the heat used for the process of evaporation, and the system of both vessels is heating up. Temperature difference, heat flow and vapour mass flow increase as well.
(2) Cooling: the vessels are disconnected from the expansion machine and the valve between the two vessels is still closed. The solution vessel is connected to the bath of 120°C and the water vessel to the bath of 40°C. This phase of the process is very short (around 1 s) and can barely be seen in the diagram. In this case, both vessels are cooled until the vapour pressures are equal.
(3) Charging: the valve between the two vessels is opened. Water vapour desorbs out of the solution and is condensed in the water vessel. In the beginning, the water temperature decreases very quickly, since the temperature difference to the heat sink is large. The temperature of the solution is first higher than the 'heat source' of 120°C, and the solution is cooled by the 'heat source' in addition to being cooled by the process of desorption. When the solution has reached a lower temperature than the heat source, this heat is given back to the solution. After this first period, the water temperature continues to decrease more

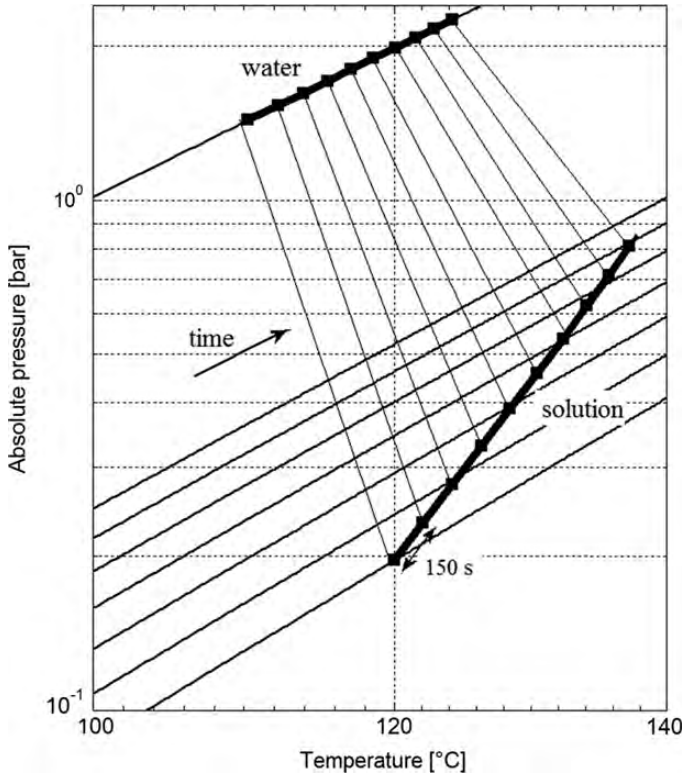

Figure 3. *Raoult plot: close-up discharging.*

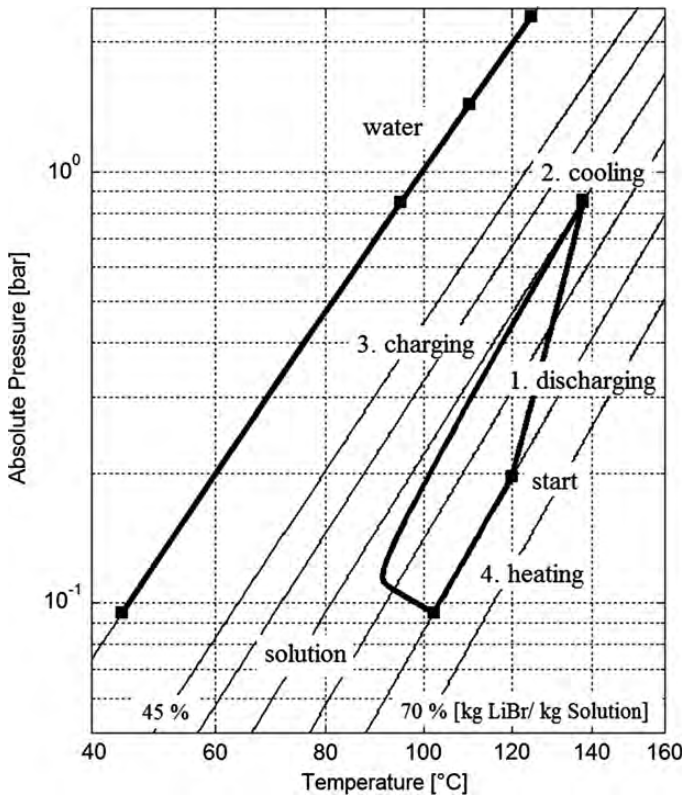

Figure 4. *Raoult plot: full cycle process.*

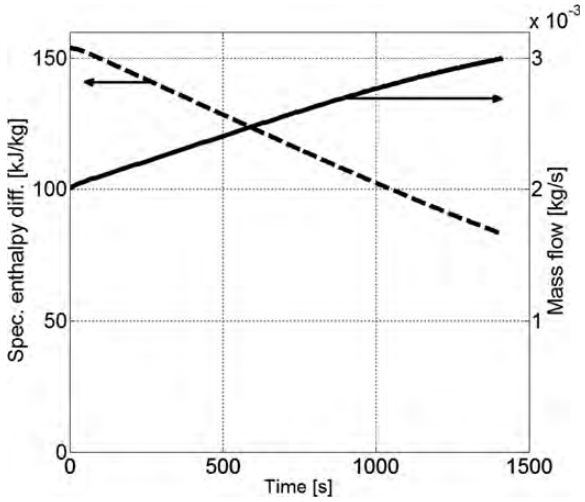

Figure 5. *Vapour mass flow $\dot{m}_{vap}$ and specific enthalpy difference over the turbine $h_{in} - h_{out}$.*

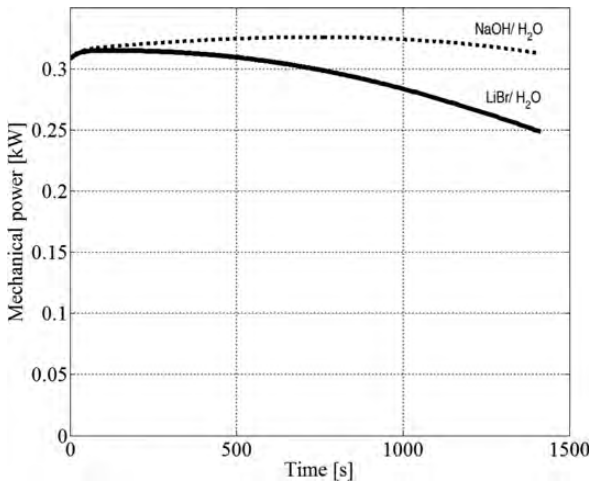

Figure 6. *Mechanical power output $\dot{W}$.*

slowly, whereas the solution temperature increases after going through a minimum. When the initial mass fraction of the solution is reached, the valve is closed.

(4) Heating: the two vessels are heated until both temperatures have reached the initial values from the beginning. At the end, the process is prepared to start again.

Figure 3 depicts a Raoult plot for the discharge phase only. The vapour pressure is plotted over the temperature. From one vapour pressure line to the neighbouring one, the change is an addition of 700 g water to the solution vessel. This is significant for the process, since the absorbed water mass or vapour mass flow relates to the work output of the expansion machine. In addition, the time has been included in the diagram: every 150 s are marked by two little squares. The thin

lines between each pair of squares show the relationship between evaporator and absorber. The vapour pressures of solution and water increase because the temperatures increase. In addition to this, the pressure over the solution increases, because it becomes more and more diluted and the vapour pressure depression decreases. Note that the vapour pressure over the solution is lower than the water vapour pressure even though the solution temperature is higher.

In Figure 4, the full cycle process can be seen in the Raoult plot with isosteres of common mass fractions. The 'time' information is not shown here. Only the beginning of each phase is marked by two squares.

Figure 5 shows the vapour mass flow $\dot{m}_{vap}$ through the expansion machine over time and the difference in the specific enthalpy of the vapour before and after the expansion machine $h_{in} - h_{out}$. The mass flow increases since the absolute pressures and the pressure difference increases [compare also Figure 3 and Stodola equation (6)]. One aspect behind this, which can be grasped more intuitively, is that a higher pressure leads to a higher vapour density, so that more mass will fit through the given expansion machine. The specific work $h_{in} - h_{out}$ decreases since the pressure ratio p_{in}/p_{out} (or p_{water}/p_{sol}) decreases around 50%, whereas the inlet temperature increases only around 4%.

In Figure 6, it can be seen how these opposite effects lead to a stabilization of the mechanical power output $\dot{W}$, since it is the product of mass flow and specific work [compare Equation (7)]. Even though the process itself has a transient behaviour, it is possible to run it in a way that the product, the power output, is quite stable.

In the following, differences between the process behaviour with the lithium bromide solution and the sodium hydroxide solution are discussed. The resulting differences originate from the different media and initial mass fractions only.

In the beginning, the increase in the temperature of the lithium bromide solution is slightly faster than for sodium hydroxide solution. This is due to a smaller specific heat capacity c_p of aqueous lithium bromide solution [around 2 kJ/(kg K)] compared with that of the sodium hydroxide solution [around 3 kJ/(kg K)]. In the end of the discharging phase, the increase in the temperature of the sodium hydroxide solution is higher. This can be explained by the higher specific heat of the absorption of the sodium hydroxide solution in the considered range of mass fraction. Generally, the differences in temperature are marginal; however, in pressure, they are not: the vapour pressure over the sodium hydroxide solution remains lower during the discharge phase. When the same amount of water is absorbed, the vapour pressure over the lithium bromide solution changes more than that over the sodium hydroxide solution. The mechanical power output for $NaOH/H_2O$ remains even more stable than for $LiBr/H_2O$ (Figure 6).

Table 2 shows the mechanical efficiency η_{mech}, the energy density ρ_{mech} and the average mechanical power output $\overline{\dot{W}}$ for both working pairs. The mechanical efficiency η_{mech} is defined as the mechanical work output divided by the heat input during the charging phases:

Table 2. *Mechanical efficiency, energy density and average mechanical power output*

	$LiBr/H_2O$	$NaOH/H_2O$
η_{mech} (%)	4.3	4.6
ρ_{mech} (Wh/kg)	4.9	5.4
$\overline{\dot{W}}$ (W)	290	330

$$\eta_{mech} = \frac{W_{mech}}{Q_{input}}. \tag{9}$$

The energy density ρ_{mech} is calculated as the output of mechanical work divided by the mass of the diluted solution at the end of the discharging phase:

$$\rho_{mech} = \frac{W_{mech}}{m_{sol,dil}}. \tag{10}$$

The average mechanical power output $\overline{\dot{W}}$ is defined as the mechanical work output over the time needed for the discharging phase:

$$\overline{\dot{W}} = \frac{W_{mech}}{time_{disch}}. \tag{11}$$

$NaOH/H_2O$ shows better results since the mean pressure difference between solution and water vessel is higher due to a higher evaporator temperature and a higher vapour pressure depression of the solution. The differences are in the range of ~10%. Nevertheless, the working pairs behave similarly, and some other criteria for the choice of working pairs should also be considered. The results are true for this set of parameters, but do not yet represent optimal process behaviour. Also, a relatively small expansion machine efficiency of 50% is used up to now. This may fit to small powers as in the given example and as in the experiment at TU Berlin; for larger power settings, higher efficiencies would be achieved. In the practical experiment, a sliding vane expansion machine is used for first tests. It is expected that an optimization will improve all characteristic numbers.

The reversible limit for a process operated with the heat input at 120°C and the heat rejection at 40°C is $\eta_{mech,\,Carnot} = 20\%$. The irreversibilities of the process are mainly due to the expansion machine and due to the heat transfer.

5 CONCLUSIONS

A fundamental model for the simulation of the Honigmann process has been developed with the help of transient energy and mass balances for the main components. Comparative simulations for two working pairs—$LiBr/H_2O$ and $NaOH/$

H_2O—have been carried out. The results show that the choice of the working pair does have an influence on efficiency, energy density and mean power density. Another result is that it is possible to obtain a stable power output, even though the process itself is transient. Further investigations on the model and process behaviour are still necessary.

ACKNOWLEDGEMENTS

Thanks to Alexandra Mehlhase for help with Modelica-specific problems and the implementation of variable-structure models [25]. This work is being carried out within a research project funded by the DFG (Deutsche Forschungsgemeinschaft).

REFERENCES

[1] Honigmann M. Utilization of exhaust-steam. Specification forming part of Reissued Patent No. 10,675, dated 22 December 1885. Original No. 287,937, dated 6 November 1883. Application for reissue filed 6 October 1884, Serial No. 144,891. United States Patent Office.

[2] Mähr C. *Vergessene Erfindungen – Warum fährt die Natronlok nicht mehr?* DuMont Literatur und Kunst Verlag 2003 [German].

[3] Honigman's condenser for tramway engines. *Engineering* 1884;53–4.

[4] Gutermuth MF. Untersuchungen an Honigmann'schen feuerlosen Natronkesseln. *Zeitschrift des Vereines Deutscher Ingenieure* 1884;**28**:69–74, 89–95 and 109–112 [German].

[5] Gutermuth MF. Versuche an einer Personenzuglocomotive mit Honigmann'schem Natronkessel. *Zeitschrift des Vereines Deutscher Ingenieure* 1884;**28**:533–7 [German].

[6] Gutermuth MF. Das Honigmann'sche Natronverfahren. Anwendungen hoher Dampfspannungen, Verhalten verschiedener Kesselmaterialien und Betriebskosten. *Zeitschrift des Vereines Deutscher Ingenieure* 1885;**29**:101–7 [German].

[7] Honigmann's caustic soda condenser. *Engineering* 1885;225–6.

[8] Honigmann M. Storing power. Specification forming part of Letters Patent No. 333,222, dated 29 December 1885. Application filed 28 May 1885, Serial No. 166,984. United States Patent Office.

[9] Honigmann M. Method of driving steam-engines. Specification forming part of Letters Patent No. 340,718, dated 27 April 1886. Application filed 14 November 1885, Serial No. 182,794. United States Patent Office.

[10] Lamm E. Improvement in ammoniacal-gas engines. Patent No.105,581, patented 19 July 1870. United States Patent Office.

[11] D'Equevilley-Montjustin R. Method of generating steam for submarine boats. Specification of Letters Patent No. 986,373, Patented 7 March 1911. Application filed 12 May 1909, Serial No. 495,491. United States Patent Office.

[12] D'Equevilley-Montjustin R. Soda steam-generator. Specification of Letters Patent No. 1.003,095, Patented 12 September 1911. Application filed 20 March 1909, Serial No. 484,771. United States Patent Office.

[13] Isshiki N. Study on the concentration difference energy system. *J Non-Equilib Thermodyn* 1977;**2**:85–107.

[14] Isshiki N, Nikai I, Uchida H. Concentration difference energy operated power plants and media used in conjunction therewith. United States Patent, 4.122.680, Appl. No. 741.033, 1978. United States Patent Office.

[15] Isshiki N, Ogawa K, Kamoshida J. Absorption steam tricycle driven by concentrated solar heat energy. *Proceedings of 'Ab-Sorption 96'*, 17–20 September 1996, Canada, p.661–7.

[16] Jahnke A, Ziegler F, Karow M. Re-evaluation of the Honigmann-process: thermo-chemical heat store for the supply of electricity and refrigeration. *Proceedings of the Heat Powered Cycles Conference, 2009*, Berlin, Germany.

[17] Modelica. 2010. Modelica language specifications version 3.2, Copyright © 2003–2010 Modelica Association. www.modelica.org (15 April 2013, date last accessed).

[18] Dymola. Dynamic modeling laboratory, version 7.4 FD01, Copyright © Dassault Systèmes, 1992–2010, February 2011.

[19] Sigloch H. *Strömungsmaschinen: Grundlagen und Anwendungen*. Carl Hanser Verlag, München and others, 1984 [German].

[20] Chaibakhsh A, Ghaffari A. Steam turbine model. *Simul Model Practice Theory* 2008;**16**:1145–62.

[21] Strenge LIJ. Der Honigmann-Prozess als thermochemischer Energiespeicher zur Erzeugung mechanischer Arbeit aus Niedertemperaturwärme – Modellierung und Simulation in Modelica. Bachelor Thesis. Technische Universität Berlin 2011.

[22] Pátek J, Klomfar J. A computationally effective formulation of the thermodynamic properties of LiBr-H2O solutions from 273 to 500K over full composition range. *Int J Refriger* 2006;**29**:566–78.

[23] Olsson J, Jernqvist Å, Aly G. Thermophysical properties of aqueous NaOH-H_2O solutions at high concentrations. *Int J Thermophys* 1997;**18**:779–793.

[24] IAPWS 97. The International Association for the Properties of Water and Steam (IAPWS), Revised Release on the IAPWS Industrial Formulation 1997 for the Thermodynamic Properties of Water and Steam, 2007.

[25] Mehlhase A. Variation des Detaillierungsgrades während der Simulation – Detaildynamik/Varying the level of detail during simulation. ASIM Symposium, 21. *Symposium Simulationstechnik: Grundlagen, Methoden und Anwendungen in Modellbildung und Simulation*, 7–9 September 2011, Winterthur, Switzerland. http://project.zhaw.ch/de/engineering/asim (15 April 2013, date last accessed).